

Scaling of rise time of drive current on development of magneto-Rayleigh-Taylor instabilities for single-shell Z-pinches

Xiaoguang Wang(王小光), Guanqiong Wang(王冠琼), Shunkai Sun(孙顺凯), Delong Xiao(肖德龙), Ning Ding(丁宁), Chongyang Mao(毛重阳), and Xiaojian Shu(束小建)

Citation: Chin. Phys. B, 2022, 31 (**2**): 025203. DOI: 10.1088/1674-1056/ac1fd9
Journal homepage: http://cpb.iphy.ac.cn; http://iopscience.iop.org/cpb

What follows is a list of articles you may be interested in

Simulations on the multi-shell target ignition driven by radiation pulse in Z-pinch dynamic hohlraum

Shi-Jia Chen(陈诗佳), Yan-Yun Ma(马燕云), Fu-Yuan Wu(吴福源), Xiao-Hu Yang(杨晓虎), Yun Yuan(袁赟), Ye Cui(崔野), and Rafael Ramis

Chin. Phys. B, 2021, 30 (**11**): 115201. DOI: 10.1088/1674-1056/ac01c2

Numerical study on magneto-Rayleigh-Taylor instabilities for thin liner implosions on the primary test stand facility

Xiao-Guang Wang(王小光), Shun-Kai Sun(孙顺凯), De-Long Xiao(肖德龙), Guan-Qiong Wang(王冠琼), Yang Zhang(张扬), Shao-Tong Zhou(周少彤), Xiao-Dong Ren(任晓东), Qiang Xu(徐强), Xian-Bin Huang(黄显宾), Ning Ding(丁宁), Xiao-Jian Shu(束小建)

Chin. Phys. B, 2019, 28 (**3**): 035201. DOI: 10.1088/1674-1056/28/3/035201

Preliminary investigation on electrothermal instabilities in early phases of cylindrical foil implosions on primary test stand facility

Guanqiong Wang(王冠琼), Delong Xiao(肖德龙), Jiakun Dan(但家坤), Yang Zhang(张扬), Ning Ding(丁宁), Xianbin Huang(黄显宾), Xiaoguang Wang(王小光), Shunkai Sun(孙顺凯), Chuang Xue(薛创), Xiaojian Shu(束小建)

Chin. Phys. B, 2019, 28 (**2**): 025203. DOI: 10.1088/1674-1056/28/2/025203

Upstream ion wave excitation in an ion-beam-plasma system

Kai-Yang Yi(弋开阳), Jin-Xiu Ma(马锦秀), Zi-An Wei(卫子安), Zheng-Yuan Li(李政元)

Chin. Phys. B, 2018, 27 (**5**): 055201. DOI: 10.1088/1674-1056/27/5/055201

Analytical studies on the evolution processes of rarefied deuterium plasma shell Z-pinch by PIC and MHD simulations

Cheng Ning(宁成), Xiao-Qiang Zhang(张小强), Yang Zhang(张扬), Shun-Kai Sun(孙顺凯), Chuang Xue(薛创), Zhi-Xing Feng(丰志兴), Bai-Wen Li(李百文)

Chin. Phys. B, 2018, 27 (**2**): 025207. DOI: 10.1088/1674-1056/27/2/025207

Scaling of rise time of drive current on development of magneto-Rayleigh–Taylor instabilities for single-shell *Z*-pinches

Xiaoguang Wang(王小光), Guanqiong Wang(王冠琼), Shunkai Sun(孙顺凯), Delong Xiao(肖德龙)†, Ning Ding(丁宁), Chongyang Mao(毛重阳), and Xiaojian Shu(束小建)

Institute of Applied Physics and Computational Mathematics, Beijing 100094, *China*

(Received 19 April 2021; revised manuscript received 22 July 2021; accepted manuscript online 22 August 2021)

In fast *Z*-pinches, rise time of drive current plays an important role in development of magneto-Rayleigh–Taylor (MRT) instabilities. It is essential for applications of *Z*-pinch dynamic hohlraum (ZPDH), which could be used for driving inertial confinement fusion (ICF), to understand the scaling of rise time on MRTs. Therefore, a theoretical model for nonlinear development of MRTs is developed according to the numerical analysis. It is found from the model that the implosion distance $L = r_0 - r_{mc}$ determines the development of MRTs, where r_0 is the initial radius and r_{mc} is the position of the accelerating shell. The current rise time τ would affect the MRT development because of its strong coupling with the r_0. The amplitude of MRTs would increase with the rise time linearly if an implosion velocity is specified. The effects of the rise time on MRT, in addition, are studied by numerical simulation. The results are consistent with those of the theoretical model very well. Finally, the scaling of the rise time on amplitude of MRTs is obtained for a specified implosion velocity by the theoretical model and numerical simulations.

Keywords: magneto-Rayleigh–Taylor instability, rise time, *Z*-pinch, magnetohydrodynamic

PACS: 52.57.Fg, 52.59.Qy, 52.30.Cv **DOI:** 10.1088/1674-1056/ac1fd9

1. Introduction

The *Z*-pinch dynamic hohlraum (ZPDH) is one of potential configurations to achieve fusion ignition.[1–7] It is formed after an annular high-atomic-number *Z*-pinch plasma is accelerated by an axial current and then impacts onto a low density foam cylinder.[2,8–11] A high opacity *Z*-pinch plasma can trap the radiation generated in the impaction process and acts as a hohlraum wall, and its ability to reduce the radiation loss to vacuum is vital for applications of inertial confinement fusion (ICF).

Magneto-Rayleigh–Taylor (MRT) instabilities will occur at outer surface of a *Z*-pinch plasma when it is accelerated by the azimuthal magnetic field produced by the axial drive current.[12–18] They can slow down the plasma and disturb the plasma density and momentum distributions,[13,15,19] thus weakening the radiating shock and reducing the *Z*-pinch plasma's capability of trapping x-ray radiation in the hohlraum.[20,21] Therefore, it is strongly expected that development of MRT instabilities can be controlled to an acceptable extent by appropriate measures in ZPDH driven ICF.

Peak and rise times of drive current play important roles in implosion dynamics of *Z*-pinch plasmas, as well as development of MRT instabilities.[6,15] In engineering, long rise time is preferred very much in constructing a large current pulse power generator for ICF. Therefore, effects of rise time of drive current are important topic in community of *Z*-pinch driven ICF. Recently, Slutz studied the scaling of magnetized liner inertial fusion (MagIIF) with the rise time by numerical simulation.[22] It shows that the required energy and preheat energy for a given fusion gain will increase with the rise time. In ZPDH applications, the development of MRT instabilities should be considered to determine a suitable rise time besides the overall energy balance. In this paper, we focus on the former.

Lots of works have been carried out on MRT instabilities in *Z*-pinch community.[6,15–17,23–34] In compared experiments of foil and wire-array *Z*-pinches on *Z* machine,[35] it is thought that one of possible reasons for lower stability of copper foil is a longer period for MRT developing in run-in phase compared to a wire array. The linear theoretical analysis of single mode indicates that the perturbation amplitude of MRT is only related to the implosion distance over which the accelerating plasma shell takes.[36,37] Some experiments show that large radius *Z*-pinches are inherently susceptible to the MRT instability.[38,39] A long rise time is required for matching the large radius because of their strong coupling. Therefore, the long rise time would result in more unstable MRTs. However, the conclusions mostly result from observing indirect parameters, such as the peak and pulse width of x-ray radiation. The scaling of rise time on the nonlinear development of MRTs is still an interesting topic for single shell implosion.

Therefore, effects of implosion parameters on the nonlinear development of MRT instabilities and their dependence on the rise time of drive current are studied in the run-in phase of a single shell implosion by theoretical analysis and simulation. It is found that the amplitude of MRTs before stagnation will

†Corresponding author. E-mail: xiao_delong@iapcm.ac.cn

© 2022 Chinese Physical Society and IOP Publishing Ltd

increase with the rise time linearly if an implosion velocity is specified. Finally, a scaling of the rise time on MRTs is given.

This paper is organized as follows. In Section 2, we introduce the physical model for numerical simulation. Firstly, the development characteristic of MRTs is numerically analyzed in Section 3. Then, in Section 4, a theoretical model for nonlinear development of MRTs in thin shell implosion is developed according to the numerical analysis. Section 5 presents the results of simulation about the effect of rise time on MRTs, which are consistent with the theoretical model. Section 6 gives the conclusions.

2. Physical models

The MRT instability in r–z cross section is taken into account, because it is most severe in the run-in phase of the plasma implosion. Although wire array loads are generally employed so far, they may transform into plasma shells with load current larger than 30–50 MA due to the increase of wire diameter and decrease of inter-wire gaps.[40] The process of early plasma formation and ablation of the wire array are beyond the scope of this article. We focus on the run-in phase in Z-pinches. Therefore, a plasma shell of uniform density is taken as the initial condition in our study. The control equations are compressible resistive magnetohydrodynamic (MHD) equations, including the continuity equation, the momentum equation, the energy equation and the magnetic field equation, which are written as follows:

$$\frac{\partial \rho}{\partial t}+\nabla\cdot(\rho \boldsymbol{v})=0, \tag{1}$$

$$\rho\frac{\partial \boldsymbol{v}}{\partial t}+\rho \boldsymbol{v}\cdot\nabla \boldsymbol{v}+\frac{1}{4\pi}\boldsymbol{B}\times(\nabla\times\boldsymbol{B})+\nabla p=0, \tag{2}$$

$$\frac{\partial \varepsilon}{\partial t}+\boldsymbol{v}\cdot\nabla\varepsilon+(p+\varepsilon)\nabla\cdot\boldsymbol{v}=\nabla\cdot\boldsymbol{F}_{\rm c}+(\eta\cdot\boldsymbol{J})\cdot\boldsymbol{J}, \tag{3}$$

$$\frac{\partial \boldsymbol{B}}{\partial t}+\nabla\times(-\boldsymbol{v}\times\boldsymbol{B})=-\nabla\times(c\eta\cdot\boldsymbol{J}), \tag{4}$$

where ρ is the mass density, $\boldsymbol{v}$ is the velocity, $\boldsymbol{B}$ is the magnetic field, $\boldsymbol{J}$ is the current density, η is the resistivity, c is the speed of light in vacuum, p is the pressure, and ε is the internal energy. The limited energy flux

$$\boldsymbol{F}_{\rm c}=\frac{F_{\rm sat}}{F_{\rm sat}+|F_{\rm class}|}\boldsymbol{F}_{\rm class} \tag{5}$$

is utilized in the energy equations, and the classical energy flux is

$$\boldsymbol{F}_{\rm class}=\kappa_{\rm par}\boldsymbol{b}(\boldsymbol{b}\cdot\nabla T)+\kappa_{\rm per}[\nabla T-\boldsymbol{b}(\boldsymbol{b}\cdot\nabla T)], \tag{6}$$

where T is the temperature, $\kappa_{\rm par}$ and $\kappa_{\rm per}$ are the parallel and normal thermal conductivity coefficients respectively, $\boldsymbol{b}$ is the unit vector along the $\boldsymbol{B}$. The saturated thermal conduction flux is $F_{\rm sat}=5\varphi\rho c_{\rm io}^3$ with $c_{\rm io}$ being the isothermal speed of sound and $\varphi<1$ a free parameter. Typically, the plasma temperature is from 1 eV to 100 eV, and the density is tens of mg/cm^3 in the run-in phase. Therefore, the Braginskii heat conductivity coefficients and the Spitzer resistivity are employed in the model.[41] The ideal equation of state is utilized to close the MHD equations, where the adiabatic index $\Gamma=1.4$. The effective ionization $Z_{\rm eff}=5$ is employed in this study. The temperature T is calculated by $p=(Z_{\rm eff}+1)n_{\rm i}k_{\rm B}T$, where $k_{\rm B}$ is the Boltzmann constant and $n_{\rm i}$ is the ion number density. In our model we neglect radiation loss for simplicity because it is relatively small compared to the material energy (kinetic energy plus internal energy) of the plasma in the run-in phase. This approximation will not result in the severe variation of the implosion dynamics and the corresponding MRT development.

The azimuthal magnetic field at the outer boundary is

$$B_{\theta\rm b}=\frac{2}{c}\frac{I(t)}{r_{\rm b}}, \tag{7}$$

where $I(t)$ is the drive current, $r_{\rm b}$ is the position of the outer boundary, and c is the speed of light in vacuum. In experiments, drive currents are determined by both the pulse power generator and the plasma impedance in implosion because they are strongly coupled in Z-pinches. In order to simplify the issues and to obtain a similar implosion dynamics, the drive current used is taken as[6,15]

$$I(t)=I_{\rm pk}\sin^2\left(\frac{t\pi}{2\tau}\right), \tag{8}$$

which is similar to the experimental measurements. Here, $I_{\rm pk}$ is the current peak and τ is the rise time. The coupling of the imploding plasma to the pulse power generator is neglected. However, the plasma impedance (including the resistivity) and the current distribution are calculated consistently in the physical model. The initial current is distributed only at the outer surface of the plasma shell.

The open source code PLUTO,[42] which has been successfully used for simulating MRT instabilities, is utilized to solve the above equations in thin aluminum liner experiments on the 7–8 MA facility.[43]

The thin shell model[6,15] is a commonly used approximation for the Z-pinch implosions without considering the 2D phenomena. In the model, the dimensionless parameter

$$\xi=\frac{I_{\rm pk}^2\tau^2}{cm_{\rm l}r_0^2} \tag{9}$$

is the peak of the normalized acceleration, which determine the imploding dynamic with the current shape together. Here $m_{\rm l}$ is the mass per unit length of the plasma shell and r_0 is the initial radius. The parameter ξ is termed as pinch constant in this paper.

It is challenging to distinguish the effect of the rise time from the other parameters because they are strongly coupled in Z-pinch implosions. For example, the rise time τ would increase with the initial radius r_0 if the pinch constant ξ is kept constant. We address this issue by developing a theoretical model and numerically studying the effects of the rise time on MRT instabilities in a similar Z-pinch dynamic system.

Typically, the plasma temperature is ~ 100 eV, and the density is tens of mg/cm^3 in the run-in phase of Z-pinch implosions. The magnetic Reynold number $R_{\rm m} = v_A l_0/\eta \sim 100$ and the Peclet number $P_{\rm t} = l_0 v/\kappa_{\rm per} \sim 10^{18}$ under the conditions, where ρ_0 is the initial density, $l_0 \sim 1.0$ cm is the characteristic scale, and $v_{\rm A} = \sqrt{B_0^2/8\pi\rho_0}$ is the Alfven velocity. The resistivity and thermal conduction could be ignored in Eqs. (1)–(4). Then the control equations will be reduced to ideal magnetohydrodynamic equations. The initial velocity is zero in our simulations. The Z-pinch implosions will be in Euler similarity according to Eqs. (6)–(8) and (11) in Ref. [44] if the acceleration $g(t)$ of the plasma shell. The initial density profile and pressure profiles, in addition, are identical. Therefore, same pinch constants ξ and current shapes $I(t)/I_{\rm pk}$ are provided in our simulations to get the identical acceleration. The initial plasma temperature and density are both uniform for the same pressure profile. The original width of plasma δr_0 are 0.1 cm for all the cases, which leads to $r_0/\delta r_0$ 10 in our simulations. The initial temperature is 10000 K in our simulations.[45] Note that the temperature is involved in our simulations for calculating the resistivity η, which determines the current skin depth $\lambda_{\rm skin}$. Usually, $\lambda_{\rm skin}$ is much smaller than l_0 so that the dynamics are still similar for MRT instabilities. We make $\xi = 5.0$ in simulations for obtaining the optimized implosion kinetic energy.

The perturbation amplitude of MRT instabilities is calculated by

$$A = \sqrt{\sum A_i^2}, \tag{10}$$

where A_i is the amplitude of each mode from Fourier analysis. According to Ref. [46], the perturbation spectrum is analyzed by calculating the radial density integral and subtracting its mean:

$$\begin{aligned} H(z) &= \frac{(\int \rho(r,z)\, r\,{\rm d}r) - \bar{H}}{\rho_{\rm m} r_{\rm mc}}, \\ \bar{H} &= \frac{\int \rho(r,z)\, r\,{\rm d}r\,{\rm d}z}{\int {\rm d}z}, \\ r_{\rm mc} &= \frac{\int\int \rho r^2\,{\rm d}z\,{\rm d}r}{\int\int \rho r\,{\rm d}z\,{\rm d}r}, \end{aligned} \tag{11}$$

where the density integral is divided by the max density $\rho_{\rm m} = \max\left[\int \rho(r,z)\,{\rm d}z/l\right]_r$ and the position of plasma shell $r_{\rm mc}$, in order to obtain a quantity with units of length. We define the radial center of mass as the position of the accelerating plasma shell as expressed by Eq. (11).

3. Development characteristics of MRT

In order to develop a theoretical model of MRTs, the development characteristics of MRT is firstly analyzed in a single shell Z-pinch by simulation. A plasma shell, with temperature 10000 K and density 0.41 mg/cm^3, is taken as the initial load.[47] The original shell width δr_0 is 0.1 cm. The initial radius $r_0 = 2.0$ cm, $I_{\rm pk} = 10$ MA, $m_{\rm l} = 0.5$ mg/cm and $\tau = 100$ ns, which make $\xi = 5.0$. We simulate the MRT development by seeding 0.5% random density perturbation initially. Figure 1 shows the perturbation amplitude and the dominant wavelength (at which the amplitude is the largest in the spectrum) as a function of the normalized time. The decrease of perturbation amplitude before acceleration is mainly due to the plasma expansion. After that, it begins to grow exponentially in the run-in phase, which is in agreement with the aluminum foil experiments on the MAIZE machine at University of Manchester[48] and on the pulse power generator at CAEP.[43]

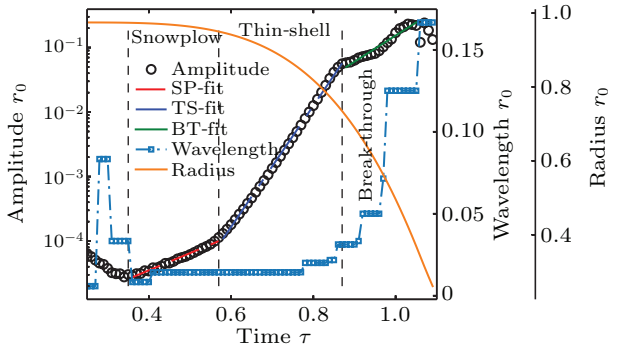


Fig. 1. The perturbation amplitude (circle) and dominant wavelength (square-dot-dashed line) of the MRT instability as a function of time for $r_0 = 2.0$ cm, $I_{\rm pk} = 10$ MA, $m_{\rm l} = 0.5$ mg/cm and $\tau = 100$ ns. The dot-dashed (red), dashed (blue) and solid (green) lines present the fitting results by $\exp(\gamma t_{\rm n})$ in the snowplow, thin-shell and break-through regimes, respectively.

We divide the run-in phase into three regimes according to the perturbation development and implosion characteristics: the snowplow regime, the thin-shell regime and the break-through regime, as shown in Figs. 1 and 2. We obtain the growth rates γ (normalized to $1/\tau$) of the perturbation, which are 6.3, 21.7, and 7.0 in different regimes, respectively, by fitting the simulation data with $\exp(\gamma t_{\rm n})$ function where $t_{\rm n} = t/\tau$ is the normalized time. In the snowplow regime, the magnetic fields accelerate and sweep the plasma like a piston at the interface as shown in Figs. 2(a) and 2(d) when the skin depth is much smaller than the initial width of the plasma δr_0. The growth rate is small due to the stabilization of accretion effects and smaller acceleration at the early time. The implosion will be in the thin-shell regime after the magnetic piston goes about δr_0, i.e., sweeping all of the plasma shell. It is found from Fig. 2(e) that the width of the plasma δr is approximate to current skin depth $\lambda_{\rm skin}$ in thin-shell regime. The growth rate becomes larger. However, the perturbation amplitude of the MRT instability is smaller than its dominant wavelength, which is almost constant in the two regimes. Namely,

the development is in linear approximately. The skin depth is about 260 μm, which is also the characteristic scales of magnetic field and density profile. The dominant wavelength is around 400 μm. The modes with the wavelength smaller than skin depth are stabilized possibly by the gradients of density and magnetic field. It is inferred that the dominant wavelength is affected by the skin depth in snow-plow and thin-shell regimes.

The magnetic field would break and penetrate through the plasma shell when the perturbation amplitude develops comparable to or larger than the width of plasm shell δr, which is approximate to the skin depth. Then, the implosion goes into the break-through regime. The amplitude is also comparable to and larger than the dominant wavelength. Under the condition, the development of MRTs will be dominated by nonlinear coupling. It can be observed from Fig. 2(c), where bubble merging occurs associating with field breaking through. The dominant wavelength increases with the amplitude dramatically as shown in Fig. 1, which means that the multi-mode development of MRTs may be in bubble-merger regime (or in self-similar growth).[49–51]

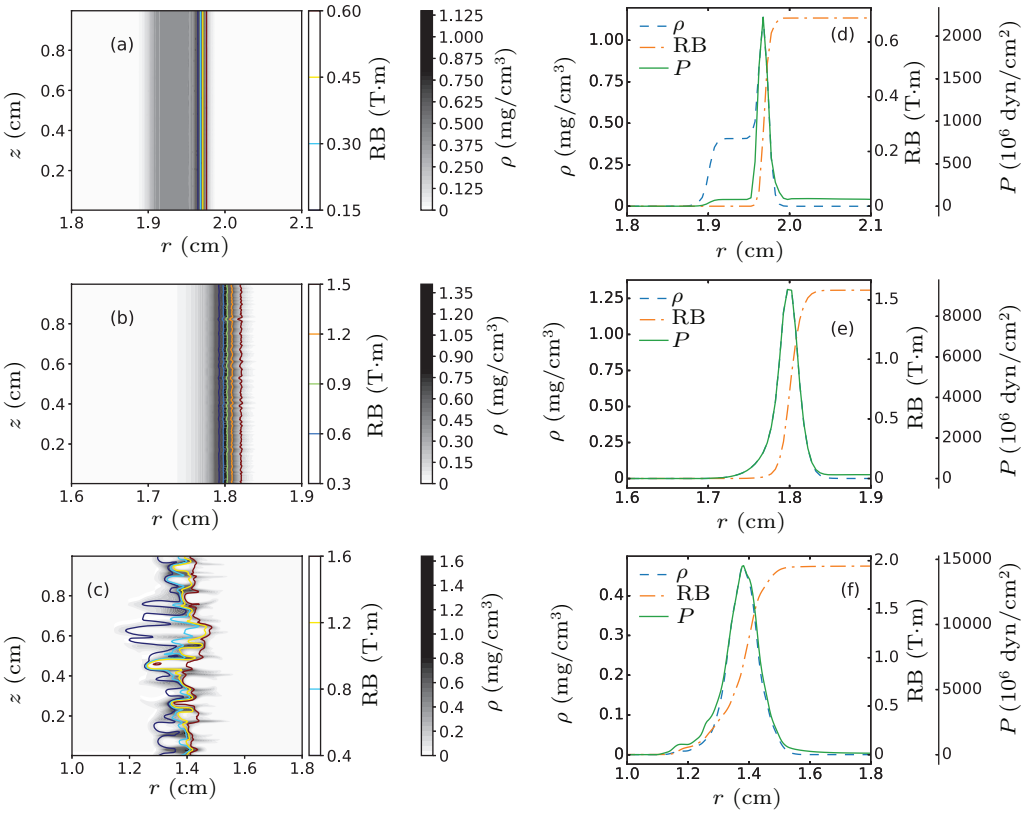


Fig. 2. Distributions of the plasma density ρ (gray map) and the RB $= B_\theta r$ (color contour lines) at (a) $t = 0.4$ (snow-plow), (b) $t = 0.7$ (thin-shell) and (c) $t = 0.9$ (break-through), (d)–(f) the radial profiles of the ρ, RB and pressure P by averaging along z direction corresponding to (a)–(c), respectively. It can be found from (e) that the skin depth is $\lambda_{\rm skin} \sim 263$ μm.

4. Model for MRT development

According to the development characteristics, we develop a model for MRT development in thin shell implosion to obtain the scaling of rise time on MRTs. The implosion distance is $L = r_0 - r_{\rm mc}$, which is normalized by $L_{\rm n} = L/r_0$. The time t, velocity v and acceleration g are normalized by $t_{\rm n} = t/\tau$, $v_{\rm n} = v\tau/r_0$ and $g_{\rm n} = g\tau^2/r_0$. The wave number k and the amplitude A of MRTs are normalized by $k_{\rm n} = kr_0$ and $A_{\rm n} = A/r_0$. For the Z-pinch implosion, the RT growth function is defined as

$$f(t_{\rm n}) = \int_{t_0}^{t_{\rm n}} \sqrt{g_{\rm n}(t')}\,{\rm d}t'. \tag{12}$$

As shown in Section 3, the amplitude is smaller than the dominant wavelength in snow-plow and thin-shell regimes. In addition, the dominant wavelength is almost constant. Thus the MRT instability grows approximately in linearity for most period in the two regimes. Then its amplitude is

$$A_{\rm n} = A_{\rm n0} \exp\left\{\sqrt{k_{\rm n}} f(t_{\rm n})\right\}. \tag{13}$$

The approximate solutions of the snow-plow model with drive current shape $\sin^2(t\pi/2)$ are[15]

$$L_{\rm n} = \frac{\pi^2}{4}\sqrt{\frac{\xi\delta r_0}{30 r_0}}\,t_{\rm n}^3 = \frac{1}{3}v_{\rm n}t_{\rm n},$$
$$g_{\rm n}(t_{\rm n}) = \frac{3\pi^2}{2}\sqrt{\frac{\xi\delta r_0}{30 r_0}}\,t_{\rm n} \tag{14}$$

for $L_{\rm n} < 1/3$. Substituting Eqs. (13) and (15) into Eq. (14), the amplitude of MRTs in the snowplow regime can be approxi-

mately written as

$$\begin{aligned} A_{\rm n} &= A_{\rm n0}\exp\left\{\sqrt{\frac{2k_{\rm n}\pi^2}{3}\sqrt{\frac{\xi\delta r_0}{30r_0}}t_{\rm n}^{3/2}}\right\} \\ &= A_{\rm n0}\exp\left\{\left(\frac{16k_{\rm n}L_{\rm n}}{3}\right)^{1/2}\right\} \\ &= A_{\rm n0}\exp\left\{\frac{4}{3}\left(k_{\rm n}v_{\rm n}t_{\rm n}\right)^{1/2}\right\}. \end{aligned} \tag{15}$$

The approximate solution of the thin-shell is[6,15]

$$\begin{aligned} L_{\rm n} &= \frac{\xi\pi^4}{480}t_{\rm n}^6 = \frac{1}{6}v_{\rm n}t_{\rm n}, \\ g_{\rm n}(t_{\rm n}) &= \frac{\xi\pi^4}{16}t_{\rm n}^4. \end{aligned} \tag{16}$$

According to Eqs. (13), (14) and (17), the amplitude of MRTs in the thin-shell regime is

$$\begin{aligned} A_{\rm n} &= A_{\rm ts}\exp\left\{\frac{1}{3}\sqrt{k_{\rm n}\frac{\xi\pi^4}{16}}t_{\rm n}^3\right\} \\ &= A_{\rm ts}\exp\left\{\left(\frac{10k_{\rm n}L_{\rm n}}{3}\right)^{1/2}\right\} \\ &= A_{\rm ts}\exp\left\{\left(\frac{5}{9}k_{\rm n}v_{\rm n}t_{\rm n}\right)^{1/2}\right\}, \end{aligned} \tag{17}$$

where $A_{\rm ts}$ is the amplitude at the beginning of the thin-shell regime.

The multi-mode development of MRTs in the break-through regime is in self-similar growth. We estimate the bubble amplitude of the MRTs by utilizing the multimode turbulence mix width equation[14,52]

$$A_{\rm n} = A_{\rm nl} + \alpha f^2(t_{\rm n}), \tag{18}$$

which is based on self-similar growth or bubble merger models. Here, α is a dimensionless coefficient, $\alpha = 0.06$ for Atwood number $A_{\rm twood} = 1.0$, and $A_{\rm nl}$ is the nonlinear saturated amplitude beyond which the MRT instability would go into self-similar growth. Inserting Eqs. (12) and (16) into Eq. (18) yields the amplitude of MRTs:

$$\begin{aligned} A_{\rm n} &= A_{\rm nl} + \frac{\alpha\xi\pi^4}{144}t_{\rm n}^6 = A_{\rm nl} + \frac{10\alpha}{3}L_{\rm n} \\ &= A_{\rm nl} + \frac{5\alpha}{9}v_{\rm n}t_{\rm n}. \end{aligned} \tag{19}$$

Finally, the development of MRTs can be expressed as

$$A_{\rm n} = A_{\rm n0}\exp\left\{\sqrt{\frac{2k_{\rm n}\pi^2}{3}\sqrt{\frac{\xi\delta r_0}{30r_0}}t_{\rm n}^{3/2}}\right\}, \ ({\rm SP})$$

$$A_{\rm n} = A_{\rm ts}\exp\left\{\frac{1}{3}\sqrt{k\frac{\xi\pi^4}{16}}(t^3 - t_{\rm ts}^3)\right\}, \ ({\rm TS})$$

$$A_{\rm n} = A_{\rm nl} + \frac{\alpha\xi\pi^4}{144}\left(t_{\rm n}^6 - t_{\rm nl}^6\right), \ ({\rm BT}) \tag{20}$$

or

$$\begin{aligned} A_{\rm n} &= A_{\rm n0}\exp\left\{\left(\frac{16k_{\rm n}L_{\rm n}}{3}\right)^{\frac{1}{2}}\right\} \\ &= A_{\rm n0}\exp\left\{\frac{4}{3}\left(k_{\rm n}v_{\rm n}t_{\rm n}\right)^{\frac{1}{2}}\right\}, \ (L_{\rm n} < \delta r/r_0); \\ A_{\rm n} &= A_{\rm ts}\exp\left\{\left[\frac{10k_{\rm n}\left(L_{\rm n} - \delta r_0/r_0\right)}{3}\right]^{1/2}\right\} \\ &= A_{\rm ts}\exp\left\{\left(\frac{5}{9}k_{\rm n}v_{\rm n}t_{\rm n} - \frac{\xi\pi^4}{480}t_{\rm ts}^6\right)^{1/2}\right\}, \\ &\quad (\delta r/r_0 < L_{\rm n} < L_{\rm nl}); \\ A_{\rm n} &= A_{\rm nl} + \frac{10\alpha}{3}\left(L_{\rm n} - L_{\rm nl}\right) \\ &= A_{\rm nl} + \frac{5\alpha}{9}v_{\rm n}t_{\rm n} - \frac{\alpha_0\xi\pi^4}{144}t_{\rm nl}^6, \ (L_{\rm n} > L_{\rm nl}); \end{aligned} \tag{21}$$

where $t_{\rm ts}$ is the time at the beginning of the thin-shell regime, $L_{\rm nl}$ is the implosion distance where the perturbation amplitude reaches $A_{\rm nl}$, and $t_{\rm nl}$ is the corresponding normalized time.

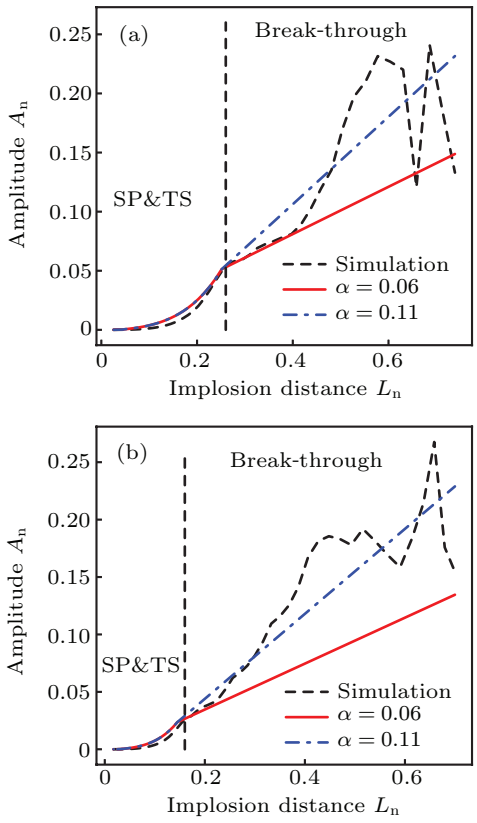


Fig. 3. The perturbation amplitudes from Fourier analysis of simulation data (dashed line) and theoretical estimation (solid and dot-dashed lines) as a function of implosion distance for $r_0 = 2.0$ cm (a) and $r_0 = 3.0$ cm (b) with $\tau = 100$ ns, $I_{\rm pk} = 10$ MA and $\xi = 5.0$.

The comparison between the theoretical and simulated results is given for the implosions with $r_0 = 2.0$ cm and $r_0 = 3.0$ cm for $\tau = 100$ ns, $I_{\rm pk} = 10$ MA and $\xi = 5.0$ in Fig. 3. The implosion distance L is given by the simulation. The simulated

results indicate the dominant wavelength is around 400 μm in snow-plow and thin-shell regimes. Thus, the single modes with $k_n = 42$ for $r_0 = 2.0$ cm and $k_n = 70$ for $r_0 = 3.0$ cm are estimated by the theoretical model. The initial amplitude is about $2.0 \times 10^{-4} r_0$. It shows that the model is in agreement with the simulation very well in the snowplow and thin-shell regime. It is also a good approximation at the beginning of the break-through regime. Then, the simulations are beyond the theoretical results. This is because the dominant wavelength becomes larger than the amplitude again in some period due to dramatic bubble merging as shown by Figs. 1 and 2. As a result, the MRT development becomes approximately exponential in $f(t_n)$ again at that time. Similar phenomena were observed in aluminum foil experiments.[48,53] The model also could estimate the amplitude of MRTs qualitatively in the regime if the α is multiplied by a coefficient ~ 1.85, i.e., making $\alpha = 0.11$, as shown by the dash-dotted lines in Fig. 3.

It is found from the model that the development of MRTs is only related to the implosion distance L (or the initial radius). Usually, the nonlinear amplitude A_{nl} is hundreds of micrometers as mentioned in Section 3. The implosion distance L is taken from mm to cm for the thin shell implosion, which is much larger than A_{nl}. Therefore, the implosion distance in the break-through regime will determine the development of the MRTs, especially for the large radius r_0. From another perspective, the perturbation amplitude increases linearly with the implosion time t for identical implosion velocity v. The scaling

$$A \cong \frac{5}{9} \alpha v t_n \tau \tag{22}$$

could be obtained from Eq. (21) with $A_n = A/r_0$ and $v_n = v\tau/r_0$. Usually, t_n is constant for the same pinch constant ξ and normalized implosion distance L_n. The implosion time t is equal to the current rise time τ when $t_n = 1$. It is concluded from Eq. (22) that the MRT amplitude will increase linearly with the rise time τ if an implosion velocity is specified.

5. Numerical results

5.1. Effects of the implosion parameters on MRTs

The effects of the implosion parameters on the MRT development are also studied in the similar Z-pinch dynamic system by simulation according to the theoretical model in this section. Firstly, we make a research on the effect of perturbation seed. It is found that the instability amplitude of MRTs increases linearly with the initial amplitude in the thin-shell regime. Then the current peak's effect on MRT in the run-in phase is studied by changing it from 5 MA to 50 MA. The matched mass is adopted to keep the pinch constant $\xi = 5.0$. The MRT instabilities show similar development for different current peaks in our simulations. The reason is clearly such that the implosion dynamics (acceleration process) in the similar system is almost identical though the peak current is varied. However, it should be noted that the effects of current peak on the process of plasma formation are not considered in the paper, which could affect the developments of MRTs by changing the perturbation seed, the temperature and density profile.[36,54]

With other parameters corresponding to Fig. 1, effect of the current rise time τ on the development of MRTs is studied. The matched mass m_l is used to keep $\xi = 5.0$ in the simulation. It is found that the MRTs develop similarly for different rise times with the same initial radius r_0 and pinch constant ξ. Figure 4 presents that the growth rates for different rise times in the three regimes are almost identical. The different initial perturbations evolved in early expansion before the acceleration may account for the small difference. The mean growth rates γ are obtained by averaging the results in Fig. 4, which are 6.1, 20.9 and 8.3 in the three regimes, respectively.

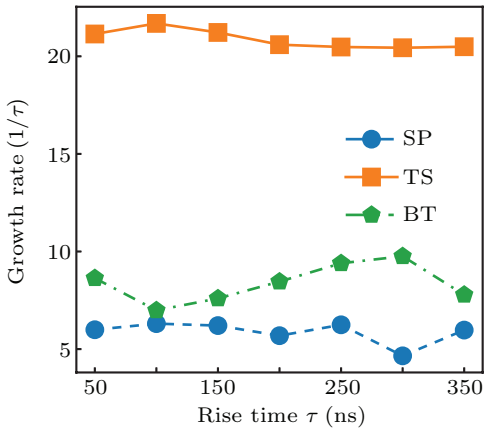


Fig. 4. With other parameters corresponding to Fig. 1, the current rise time τ is changed from 50 ns to 350 ns, and the matched masses m_l are used to keep $\xi = 5.0$. The fitting growth rates vs the rise time in the snowplow (SP), thin-shell (TS) and break-through (BT) regimes are presented.

The similar results are also found for $r_0 = 1.0$ cm and 3.0 cm as depicted in Figs. 5(a) and 5(b). However, it is found that the amplitude and dominant wavelength of MRTs before stagnation increase with the initial radius r_0 from 1.0 cm to 3.0 cm. The amplitude increases from 0.1 cm to 0.54 cm, and the dominant wavelength increases from 0.07 cm to 0.3 cm. The average growth rates γ in the snow-plow regime are 5.43 and 6.82 for $r_0 = 1.0$ and 3.0 cm. The growth rates in the thin-shell regime are 18.3 and 23.5, and the average growth rate in the break-through regime is 8.1 for $r_0 = 3.0$ cm. The development period of MRT in this regime is very short in the case of small radius $r_0 = 1.0$ cm, so the growth rate is not given. It is obvious that the initial radius r_0 of the plasma shell plays a key factor for MRT development in the Z-pinch. In other words, the implosion distance L determines the amplitude of MRTs.

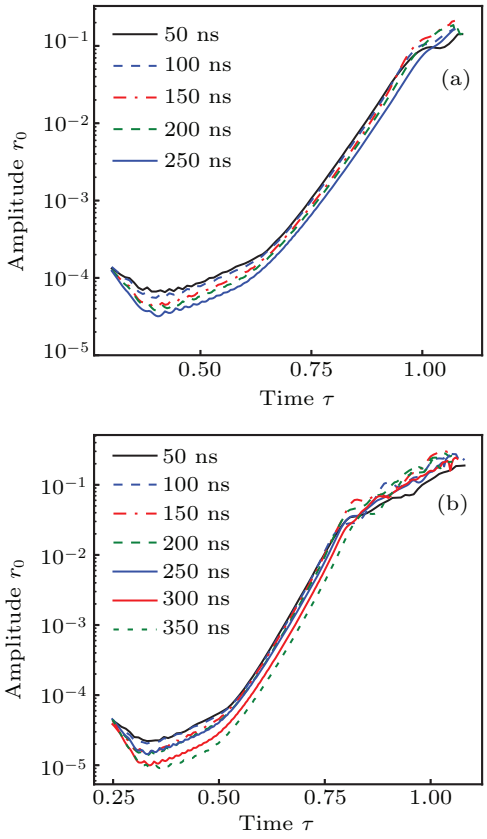


Fig. 5. The amplitude as a function of time for different current rise times τ with $r_0 = 1.0$ cm (a) and $r_0 = 3.0$ cm (b). The pinch constant is kept $\xi = 5.0$ by utilizing matched masses. The other parameters correspond to Fig. 1.

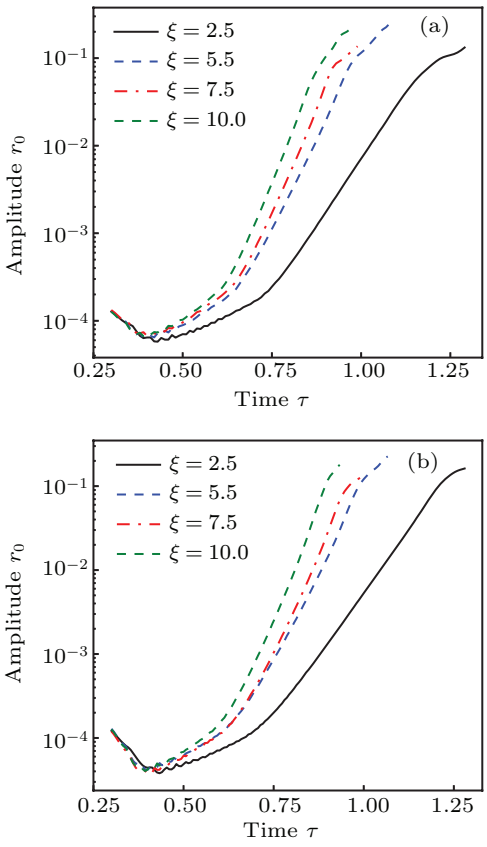


Fig. 6. (a) and (b) The perturbation amplitude as a function of time for different pinch constants with the rise times 50 ns and 150 ns, respectively. The pinch constant is changed by adjusting the mass m_1.

The effect of pinch constant is also investigated by only adjusting the mass with $I_{pk} = 10$ MA, $r_0 = 1.0$ cm and $\tau =$ 50 ns or 150 ns. Figure 6 shows the perturbation amplitude as a function of time for different pinch constants with the rise times 50 ns (Fig. 6(a)) and 150 ns (Fig. 6(b)). The growth rate γ increases with pinch constant ξ (i,e, peak of normalized acceleration) as expected. However, longer period is needed for the same implosion distance with smaller ξ. Finally, the perturbation amplitude of MRTs may be identical for the same implosion distance. Corresponding to Fig. 6, Fig. 7 shows the amplitude as a function of the implosion distance L for different pinch constants. As predicted by the theoretical model, the amplitudes are only related to the implosion distance L when ξ is larger than 2.5. It also supports that the implosion distance L plays an important role in the development of MRTs. It is demonstrated that the results are consistent with the prediction of the theoretical model very well.

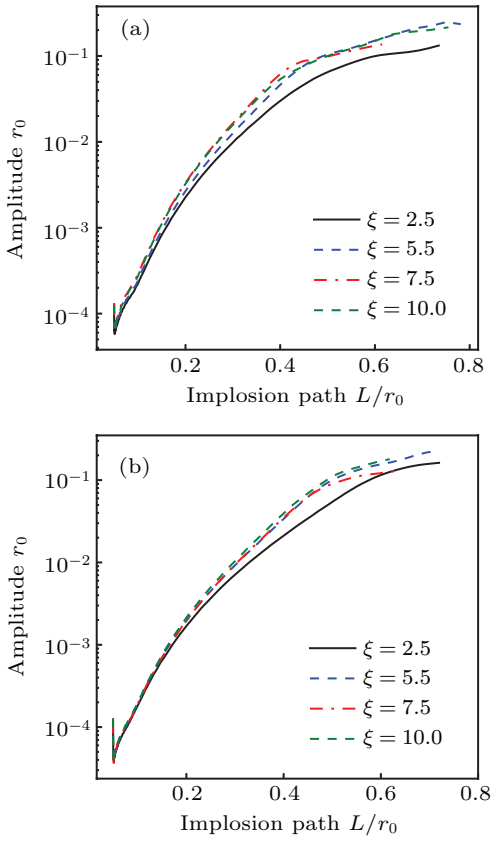


Fig. 7. Corresponding to Fig. 6, the perturbation amplitude as a function of the implosion distance L for different pinch constants with the rise times 50 ns (a) and 150 ns (b).

5.2. Scaling of rise time on MRTs

In fact, high plasma implosion velocity is needed to generate high temperature radiation for ZPDH application and others. Clearly, the implosion velocity is approximately proportional to the ratio of the initial radius to the rise time provided the same pinch constant. So longer rise time requires larger radius if the identical implosion velocity and mass m_1

are kept. Consequently, the perturbation amplitude would increase with the rise time according to the theoretical model.

In order to validate it, we also study the effect of rise time on the MRT instabilities by simulation, keeping identical pinch constant ξ, implosion velocity v and the mass per unit length m_{l}. Figure 8 presents the amplitude A_{stg} before the stagnation as a function of the rise time τ. The matched radiuses are used to keep v_{f} and ξ constant. It is found that the amplitude of MRTs increases with the rise time τ linearly, i.e., $A_{\mathrm{stg}} \propto a\tau$, where a is a coefficient in cm/μs and is about 1.63 from the result of Fourier analysis. The amplitudes of spike-bubble, which is the distance from the outmost tip of spikes to the innermost tip of bubbles, are also given, since the perturbation amplitude of Fourier analysis may not be exact enough when it is larger than the radial position of the plasma in this paper. Usually, the latter is twice the Fourier analysis or even larger.

It is obtained from the theoretical model that $a = 5\alpha v/9\tilde{1}.87$ cm/μs, where the implosion velocity $v = 30.6$ cm/μs is given by the simulation in Fig. 8. It is shown that the theoretical result agrees with the simulation very well.

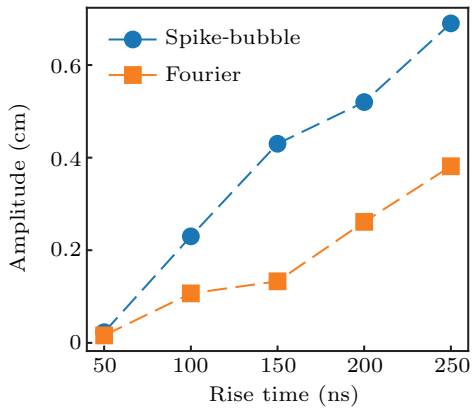


Fig. 8. The perturbation amplitude as a function of the rise time τ before stagnation. The square-dashed line is the amplitude obtained by Fourier analysis. The circle-dashed line is the spike-bubble amplitude. Note that the matched radii are used to keep v and ξ identical. The other parameters correspond to Fig. 1.

6. Conclusions

In summary, the development characteristics of MRTs are firstly analyzed by simulation for a single shell implosion. In the analysis, we divide the run-in phase into three regimes according to the perturbation characteristics and implosion dynamics: the snow-plow regime, the thin-shell regime and the break-through regime. The perturbation amplitude of MRTs grows exponentially with time in the run-in phase. It is found that the perturbation amplitude is smaller than the dominant wavelength in the snowplow and thin-shell regimes, so the development of MRTs is nearly linear. Usually, the perturbation amplitude is comparable to or larger than the dominant wavelength in the break-through regime. In addition, the dominant wavelength increases with the perturbation amplitude. The development of MRTs is in self-similar (nonlinear coupling) in this regime. However, it will return to the linear regime for some period due to dramatic bubble-merging, which leads to the dominant wavelength larger than the perturbation amplitude.

According to the numerical analysis, a theoretical model for nonlinear development of MRTs in thin shell implosion is developed. The model is in agreement with the numerical results very well in the snowplow and thin-shell regimes. In the breaking-through regime, the model could qualitatively predict the numerical results by modifying the coefficient α of RT mix width equation.

It is seen from the theoretical model that the implosion distance L determines the amplitude of MRT instabilities. The result is not affected by the pinch constants very much. The rise time, however, could also affect the MRT development because it couples with the initial radius strongly if an implosion velocity is specified. In ZPDH applications, for example, a high implosion velocity is necessary for the high temperature radiation. The long rise time will lead to large implosion distance L for keeping the high implosion velocity. Consequently, the amplitude of MRTs increases with the rise time. According to the model, the amplitude before the stagnation increase with the rise time linearly for a specified velocity. Actually, it will also be true for the Z-pinch radiation source if the high radiation power is required.

Then effects of the rise time on MRTs are also studied by simulations. The results demonstrate that implosion distance L plays a key factor in development of MRTs. The scaling of rise time on MRTs for a specified velocity is consistent with the theoretical. Finally, a scaling of rise time on MRT development $A \sim \frac{5\alpha v}{9}\tau$ is obtained by the theoretical model and simulations, where $\alpha = 0.11$.

It should be noted that the development of MRTs is more complicated in the break-through regime. At the beginning of the breakthrough regime, the RT mix width equation based on self-similar growth or bubble-merger model is a good approximation. However, the development will return to the linear growth because of dramatic bubble-merging for some period. Therefore, a better model should be developed for the breaking-through regime in future.

In addition, the effects of the peak and rise time on the process of plasma formation in the initial phase of the implosion will affect the MRT development by affecting the perturbation seed, the density profile and the plasma temperature. These issues are beyond the scope of this paper. Furthermore, only the current shape of $\sin^2(\pi t/2\tau)$ is applied in the paper. The changing of the current shape should also be considered carefully in future. The effects of equation of state and radiation would also affect the temperature of the plasmas in

simulations. As a result, the resistivity will change, leading to different skin depths and then affecting the nonlinear amplitude $A_{\rm nl}$. These issues should also be considered carefully in future.

Acknowledgements

This work was supported by the National Natural Science Foundation of China (Grant Nos. 11975057, 11605013,11775023, and 11705013).

The simulation work in our paper is mainly performed using an open code PLUTO. The authors are grateful to the contributors of the code.

References

[1] Slutz S A, Bailey J E, Chandler G A *et al.* 2003 *Phys. Plasmas* **10** 1875
[2] Sanford T W L, Lemke R W, Mock R C *et al.* 2002 *Phys. Plasmas* **9** 3573
[3] Rochau G A, Bailey J E, Chandler G A *et al.* 2007 *Plasma Phys. Control. Fusion* **49** B591
[4] Lash J S, Chandler G A, Cooper G *et al.* 2000 *Comptes Rendus de l'Académie des Sciences-Series IV-Physics* **1** 759
[5] Bailey J E, Chandler G A, Slutz S A *et al.* 2004 *Phys. Rev. Lett.* **92** 085002
[6] Haines M G 2011 *Plasma Phys. Control. Fusion* **53** 093001
[7] Ruiz C L, Cooper G W, Slutz S A *et al.* 2004 *Phys. Rev. Lett.* **93** 015001
[8] Bailey J E, Chandler G A, Mancini R. C *et al.* 2006 *Phys. Plasmas* **13** 056301
[9] Slutz S A, Peterson K J, Vesey R A *et al.* 2006 *Phys. Plasmas* **13** 102701
[10] Sanford T W L, Nash T J, Mock R C *et al.* 2006 *Phys. Plasmas* **13** 012701
[11] Rochau G A, Bailey J E, Maron Y *et al.* 2008 *Phys. Rev. Lett.* **100** 125004
[12] Winske D 1996 *Phys. Plasmas* **3** 3966
[13] Douglas M R, De Groot J S and Spielman R B 2001 *Laser Particle Beams* **19** 527
[14] Miles A R 2009 *Phys. Plasmas* **16** 032702
[15] Ryutov D D, Derzon M S and Matzen M K 2000 *Rev. Mod. Phys.* **72** 167
[16] de Grouchy P W L, Kusse B R, Banasek J *et al.* 2018 *Phys. Plasmas* **25** 072701
[17] Sun Y B and Piriz A R 2014 *Phys. Plasmas* **21** 072708
[18] Sinars D B, Slutz S A, Herrmann M C *et al.* 2010 *Phys. Rev. Lett.* **105** 185001
[19] Peterson D L, Bowers R L, Brownell J H *et al.* 1996 *Phys. Plasmas* **3** 368
[20] Peterson D L, Bowers R L, Matuska W *et al.* 1999 *Phys. Plasmas* **6** 2178
[21] Lemke R W, Bailey J E, Chandler G A *et al.* 2004 *Phys. Plasmas* **12** 012703
[22] Slutz S A 2018 *Phys. Plasmas* **25** 082707
[23] Srinivasan B and Hakim A 2018 *Phys. Plasmas* **25** 092108
[24] Weis M R, Zhang P, Lau Y Y *et al.* 2015 *Phys. Plasmas* **22** 032706
[25] Huang B, Tomizuka T, Xie B *et al.* 2013 *Phys. Plasmas* **20** 112113
[26] Zhang P, Lau Y Y, Rittersdorf I M *et al.* 2012 *Phys. Plasmas* **19** 022703
[27] Kantsyrev V L, Esaulov A A, Safronova A S *et al.* 2011 *Phys. Rev. E* **84** 046408
[28] Lau Y Y, Zier J C, Rittersdorf I M *et al.* 2011 *Phys. Rev. E* **83** 066405
[29] Zhang Y and Ding N 2008 *Chin. Phys. B* **17** 2994
[30] Zhang Y and Ding N 2006 *Phys. Plasmas* **13** 022701
[31] Sinars D B, Cuneo M E, Jones B *et al.* 2005 *Phys. Plasmas* **12** 056303
[32] Wu J, Lu Y, Sun F *et al.* 2018 *Plasma Phys. Control. Fusion* **60** 075014
[33] Duan S, Xie W, Cao J *et al.* 2018 *Phys. Plasmas* **25** 042701
[34] Yang X, Xiao D L, Ding N *et al.* 2017 *Chin. Phys. B* **26** 075202
[35] Nash T J, Deeney C, Chandler G A *et al.* 2004 *Phys. Plasmas* **11** L65
[36] Velikovich A L, Cochran F L and Davis J 1996 *Phys. Rev. Lett.* **77** 853
[37] Liberman M A, Groot J S D, Toor A *et al.* 1999 *Physics of high-density Z-pinch plasmas* (New York: Springer Science+Business Media)
[38] Deeney C, LePell P D, Failor B H *et al.* 1994 *J. Appl. Phys.* **75** 2781
[39] Sze H, Levine J. S, Banister J *et al.* 2007 *Phys. Plasmas* **14** 056307
[40] Kantsyrev V L, Chuvatin A S, Safronova A S *et al.* 2014 *Phys. Plasmas* **21** 031204
[41] Lee Y T and More R M 1984 *Phys. Fluids* **27** 1273
[42] Mignone A, Bodo G, Massaglia S *et al.* 2007 *Astrophys. J. Suppl. Ser.* **170** 228
[43] Wang X G, Sun S K, Xiao D L *et al.* 2019 *Chin. Phys. B* **28** 035201
[44] Ryutov D D 2018 *Phys. Plasmas* **25** 100501
[45] Douglas M R, Deeney C and Roderick N F 1998 *Phys. Plasmas* **5** 4183
[46] Ofer D, Alon U, Shvarts D *et al.* 1996 *Phys. Plasmas* **3** 3073
[47] Hammer J H, Eddleman J L, Springer P T *et al.* 1996 *Phys. Plasmas* **3** 2063
[48] Yager-Elorriaga D A, Steiner A M, Campbell P C *et al.* 2016 *Phys. Plasmas* **23** 124502
[49] Sharp D H 1984 *Physica D* **12** 3
[50] Youngs D L 1984 *Physica D* **12** 32
[51] Zhou Y 2017 *Phys. Rep.* **720–722** 1
[52] Dimonte G and Schneider M 1996 *Phys. Rev. E* **54** 3740
[53] Yager-Elorriaga D A, Lau Y Y, Zhang P *et al.* 2018 *Phys. Plasmas* **25** 056307
[54] Oreshkin V I, Baksht R B, Cherdizov R K *et al.* 2021 *Plasma Phys. Control. Fusion* **63** 045022